

# Micro- Macro Simulation and Experimental Investigations of Laser Remelting Al-Coatings on steel

H. Diepers, R. Prieler, G. Laschet,  
ACCESS e.V. , Intzestr.5, 52056 Aachen

C. Theiler, E. Schubert  
BIAS, Bremen

---

## Abstract

---

*Short time surface heat treatments with high energy sources generate high heating and cooling rates resulting in fine-grained and often metastable microstructures with properties substantially differing from samples after volume heat treatments. Laser remelting of Al-coatings on steel substrates leads to the formation of intermetallic Fe-Al-phases with interesting technical properties like high temperature resistance against oxidation and corrosion. However the insufficient fundamental knowledge about the correlation of process parameters, microstructures and properties at thermal gradients above  $10^3$  K/s actually prevents a technical application.*

*To overcome this problem systematic experimental investigations in the Fe-Al system were carried out and the microstructures were determined by optical microscopy and EDX analysis.*

*Within the strategy of coupled micro-macro simulation a standard thermal FE analysis is extended in order to model the influence of changing alloy composition in the melting pool. The predicted and experimental depths of the melting pool are compared as a function of the process parameters.*

*The subsequent micro simulation is based on the phase-field method, which allows to calculate the microstructure and the microsegregation profile. The special feature here is the incorporation of the phase diagram Fe-Al in the range from 75-99 at% Al.*

*The first results are compared with the experimental investigations of microstructures. They agree in orders of magnitude with the fineness of the microstructure and render their local variations.*

---

## Introduction

---

Rapid solidification processes lead to structural changes and thus material properties modifications. However, at very high cooling rates, the equilibrium models fail, e.g. due to the over-estimation of nucleation rates [1]. Rapid growth can occur during surface treatment using a laser beam. Because of its high power density, the high heating and cooling rates can be controlled and consequently thin surface layers consisting of metastable phases can be generated [2].

Fe-Al alloys possess technological characteristics such as good corrosion and oxidation resistance also at elevated temperatures as well as a stability against sulphidizing. The correlations between characteristics of heat treatments with  $dT/dt > 10^3$  K/s, the adjusting microstructures and the material properties are not known. This obstructs the technical application of such surface layers. BIAS Bremen and ACCESS Aachen coordinate their experimental and numerical work with laser remelting in the Fe-Al-system. BIAS determines the process field of a rapid laser heat treatment to generate homogeneously mixed Al-rich thin surface layers and qualify the correlating material properties. Simultaneously ACCESS simulates the evolution of the macro- and microstructure. In the following report first the experimental conditions are presented briefly. Then the thermal FE-calculation coupled with a mixture concentration approach is explained as well as the micro simulation model which is based on the phase-field approach. Experimental and numerical results are presented and discussed at the end.

---

## Laser remelting

---

The principle of laser beam remelting is sketched in Fig. 1. Sample and optics are moved relative to each other at a constant velocity. Surface treatment using a focused laser beam permits the usage of high power densities. The variation of the transversal speed  $v$ , heat input per length and interaction times can be realised.

Specimens consisting of a 2 mm thick steel sheet and a pure Al-foil of 100  $\mu\text{m}$  thickness were mechanically bonded and afterwards treated with the laser. Remelting experiments with variable transversal speeds and different laser powers have been carried out. The process field for generating surface alloys with a high and homogenous Al content and a good surface quality has been determined. The process window was defined by plotting the heat input per length (line energy) against the feed speed. Beyond its upper limit a laser-induced plasma forms, resulting in a deep Fe-rich zone. On the other hand, below this process window, no melting of iron occurs. Therefore, it can be stated that the melt pool depth is proportionally related to the interaction time (calculated from the laser beam diameter divided by transversal speed).

In order to control high Al-contents within the remelting zone, a cyclic heat treatment has been carried out, by cladding two melting tracks successively. Then we achieve simultaneously homogenous mixture and optimum penetration depth. The relations between the microstructures, the alloy composition and the process parameters are considered by adding the interaction time and the heat input per length of the two remelting tracks. Heat losses due to the temporal delay between the two tracks are ignored.

A penetration depth less than 100  $\mu\text{m}$  into Fe has been achieved by using interaction times less than 9 ms (see Fig 2). A depth up to 270  $\mu\text{m}$  requires longer interaction times. In contrast to single heat treatments, a cyclic heat treatment allows an expansion of the process window and a larger variation of the process parameters. Repeated surface treatment with constant process parameters of the 1st and 2nd melting track allow the adjustment of a high melting depth and a high Fe content (Fig. 2 on the right). Remelting with different parameters of the two tracks allows a realisation of a low melting depth and a high Al-content in the top of the surface (Fig. 2. left).

---

## Macro-Micro simulation

---

Several models couple analytical approximations of the microstructure formation with macroscopic heat balances, e.g. [3]. The approach here combines the macro simulation and a locally resolved

direct microstructure simulation [15]: In particular temperature gradient and cooling rate are locally read off from the thermal finite element calculation on component scale. They enter then with the and the Fe-content as input- parameters into the microstructure simulation.

---

### Macro simulation and mixing concentration model

---

For the macroscopic simulation we use the software package CASTS (Computer Aided Solidification TechnologieS), which solves the heat equation by a hybrid finite element/ control volume approach [4]. An advection term describes a reference system for the sample moving with the velocity  $v$  against the laser beam (Euler formalism), and leads to the heat transport equation:

$$\left( \rho c_p - L \frac{\partial f_s}{\partial T} \right) \left( \frac{\partial T}{\partial t} + v \cdot \nabla T \right) = \nabla(\lambda \nabla T),$$

where  $f_s$  is the fraction of solidified phase and  $L$  is the latent heat. An upwind formulation was implemented, which considers the different Peclet numbers in each nodal point of the computing area. The heat source of the laser beam is described as boundary condition by an elliptical Gauss normal distribution around a fixed point (as Fig. 1).

During the laser process the melting pool composition may change from pure aluminum to nearly pure iron. The melting temperatures of the two components are very different (Fe: 1534°C: Al: 655°C). A clear definition of the melting point depending on alloy composition is however necessary for the definition of the liquid/mushy/solid zones, which determine again the alloy composition. The mixing concentration model bases on the following simplifications:

- only the steady state of the remelting process is regarded.
- the melt pool is regarded as perfectly mixed.
- the phase boundary is in thermodynamic equilibrium.

The second assumption requires larger interaction times of the heat source, so that a high mixing degree is achieved due to Marangoni convection. Interaction times  $t < 5$  ms had led to strongly varying alloy compositions [15], so that in this regime the mixing concentration model will supply only rough approximations.

In our model the nodes with temperatures above the liquidus temperature  $T > T_L(c_{\text{melt}})$  are assumed to be liquid. The implemented model considers the variation of the liquidus and solidus temperatures given by the Fe-Al phase diagram (Fig. 3), which was calculated by the thermodynamic program THERMOCALC. By defining the melting pool by the liquidus isotherm, the content of remelted Fe in the melting pool is determined again. In the code this coupling is considered by an iterative loop until the suitable parameters are found. The distribution of the latent heat is then varied too due to the iteration of the solidification interval ( $T_L > T > T_S$ ) with Fe-content. Additionally this interval is projected on the feed direction in order to avoid artificial solidification zones. Finally the iterative mixing concentration model considers the temperature and concentration dependencies of thermalphysical properties on concentration, e.g. the heat conductivity, the thermal capacity and the latent heat by linear weightings according to the alloy composition. For cyclic remelting only the second remelting process is directly calculated. The first heat treatment is taken into account by using an increased starting temperature for the second heat treatment.

---

### Micro simulation

---

The microstructure evolution as free boundary problem is described by a phase-field variable coupled with a concentration field and a given temperature distribution. Since its successful numerical application to dendritic crystal growth [5], the phase-field method has been investigated and extended by many authors [e.g. 6-13]. An overview of this method gives e.g. [14]. In the following model a simplified phase-field model for solutal coupling [13] was applied and modified slightly. The governing equations for the growth of the  $\Theta$ -phase in the system Fe-Al are presented briefly here. The phase-field equation

$$\dot{\phi} = \mu \cdot \Gamma \cdot \left( \Delta \phi - \frac{36 \phi (1 - \phi) (2 - \phi)}{\delta^2} \right) + \mu \cdot [T - T_{eq}(c_l)] \cdot \frac{630 \phi^4 (1 - \phi)^4}{\delta}$$

describes the evolution of the liquid-solid (l-s) interface. The parameter  $\phi$  has the value  $\phi=1$  in the solid phase and  $\phi=0$  in the liquid phase. The solution of the phase-field equation arises in a continuous l-s transition profile of the form  $\phi(x)=\frac{1}{2} [1-\tanh(3x/\delta)]$  with the interface-thickness  $\delta$ . The velocity  $v_{int}$  of this diffuse interface follows the physics of the extended Gibbs Thomson relation known as relevant boundary condition at the l-s interface

$$v_{int} = \mu \cdot (T_{eq}(c_l) - \Gamma \cdot \kappa - T_{int}),$$

where  $v_{int}$  is controlled by the curvature  $\kappa$  and the deviation between the temperature  $T_{interface}$  and the equilibrium temperature  $T_{eq}(c_L)$ , itself depending on solute concentration at the phase boundary. The interface kinetic is linearized using the coefficient  $\mu$ . In the present model aspects of [10] are used by simple modifications (more details in [16]).

The micro simulation focuses on the  $\Theta$ -phase ( $FeAl_3$ ), i.e. on the aluminum rich section of the phase-diagram (75- 100%), see Fig. 3. The dependence  $T_{eq}(c_l)$  has been fitted by a polynomial. The Gibbs Thomson curvature coefficient  $\Gamma(\vartheta)$  is described by the fusion entropy  $\Delta S_f$ , the surface energy  $\sigma(\vartheta)$  and the angle  $\vartheta$  of the front-normal against the crystal orientation:  $\Gamma = \sigma(\vartheta) - \sigma''(\vartheta) / \Delta S_f$ . The anisotropy of the surface energy in 2-D is assumed as 4-fold:  $\sigma = \sigma_0 [1 + \varepsilon \cos 4(\vartheta - \vartheta_0)]$  with  $\varepsilon=2\%$ .  $\Delta S_f$  and  $\sigma_0$  were taken from [1] for pure aluminium.

The concentration profile is described by assuming a total concentration  $c_{tot}$  consisting of weighted liquid ( $c_l$ ) and solid contributions ( $c_s$ ),  $c_{ges} = (1 - \phi) c_l + \phi \cdot c_s$ , where the solid concentration is assumed as constant  $c_s=75\%$  and the concentration equation in the liquid reads

$$(1 - \phi) \dot{c}_l = \nabla D_l (1 - \phi) \nabla c_l + (c_l - c_s) \cdot \dot{\phi}$$

with  $D_L$  = diffusion constant in the liquid phase,  $c_l - c_s$  = difference between liquidus and solidus due to equilibrium phase diagram. Closer details are described in [16].

The heat balance is not explicitly calculated on microstructure level, since the solute diffusivity in the system differs from the thermal diffusivity by four orders of magnitude. Hence a linear temperature profile is assumed according to the macro simulation.

## Experimental results

For the evaluation only specimens after a cyclic thermal treatment are considered here. The evolving microscopic structures generally could be divided into four categories:

- I. The remelting zone is too small: Alloying by Fe-remelting is barely achieved (only in the vicinity at the Fe-Al interface).
- II. Stemlike dendritic structure (without side branching).
- III. Inhomogenous remelted tracks, which are characterized by zones of homogeneous mixing as well as a stem formation along the convection streaks.
- IV. Homogeneous mixing with high Fe content.

Of further interest here are only the structures of the category II, where the remelted zones contain up to 28 at% Fe. The stem formations grow along the temperature gradient. As characteristics of the solidification morphology the width and length were examined comparatively for four samples with constant power density (67.83 W/cm<sup>2</sup>) and variable interaction time  $\tau$ . Length and width were determined at the upper, middle and lower zones of the remelted track (see Fig. 4).

**Table 1:** Dendrite length and dendrite thickness as a function of interaction time

Interaction time	Dendrite length [ $\mu\text{m}$ ]			Dendrite thickness [ $\mu\text{m}$ ]		
	Lower zone	Middle zone	Upper zone	Lower zone	Middle zone	Upper zone

8,222 ms	7,23-13,69	5,76-16,98	6,22-14,87	0,62-1,44	0,59-1,50	0,44-1,04
8,389 ms	5,7-11,07	7,5-15,0	7,5-17,14	1,07-2,14	0,89-1,78	0,71-1,78
8,572 ms	3,29-8,64	2,56-10,31	7,23-18,65	1,18-2,18	0,85-1,75	1,64-2,63
8,842 ms	1,92-4,84	2,82-5,78		1,03-1,65	0,55-1,36	

The following tendencies are determined: The dendrite length increases with decreasing interaction time. Within a track the dendrite length of the melt pool continuously increases in the direction up to the surface. The dendrite thickness increases with increasing interaction time. Within a track the width of the stem crystals decreases from the melt pool up to the surface.

### Comparison of macro simulation and experiment

For the verification of the macro simulation the penetration depth of the melting pool into Fe and the middle concentration of the remelted Fe-Al tracks are compared with the experimental data. The parameters of the comparison in Fig. 4 are the laser power  $P = 1.73$  kW, the feed speed  $v_s = 140$  mm/s, the interaction time  $\tau = 8.389$  ms, the laser beam diameter  $d = 0.57$  mm and the aluminum layer thickness of  $100 \mu\text{m}$ . This parameter set led in the experiment to a penetration depth of  $t = 70 \mu\text{m}$  and a middle Al concentration of 80% with variations of the concentration measurements in the interval between 73 and 84 at%.

For the simulation an absorption coefficient of 33 % was assumed. The starting temperature was increased from  $20 \text{ }^\circ\text{C}$  to  $72 \text{ }^\circ\text{C}$  due to the preceding first laser treatment. Figure 4 shows the calculated temperature distribution in the cross section through the center of the pool. The drawn liquidus isotherm roughly meets the melt pool geometry of the experiment.

The macro simulation results in a penetration depth of 75 mm (=175 mm pool depth, adding the Al-thickness) while a mixing concentration of 79.2 at% Al is reached. This values correspond well with the experiment. An absorption factor of 33% was likewise assumed therefore for the following simulation series.

In Table 2 the penetration depths and mixing concentrations for the variations in line energy and interaction time are compared between simulations and experiments.

**Table 2:** Penetration depth and average concentration for experiment and macro simulation

Process parameter Power; line energy; Interaction time	experiment		Macro simulation	
	Penetration depth	mean concentration [range]	Penetration depth	mixture concentration
1,73kW; 29,82J/mm; 9,828ms	412 $\mu\text{m}$	19 [16-18] at%Al	320 mm	50 at%Al
1,73kW; 26,84J/mm; 8,842ms	160 $\mu\text{m}$	62 [60-64] at%Al	80 mm	77.9 at%Al
1,73kW; 25,47J/mm; 8,389ms	70 $\mu\text{m}$	80 [73-84] at%Al	75 mm	79.2 at%Al
1,73kW; 24,96 J/mm; 8,222ms	40 $\mu\text{m}$	80 [71-84] at%Al	70 mm	81.5 at%Al
1,73kW; 23,54 J/mm; 7,758ms	54 $\mu\text{m}$	79 [72-83] at%Al	70 mm	81 at%Al
1,6 kW; 24,82 J/mm; 8,842ms	18 $\mu\text{m}$	85 [74-97] at%Al	70 mm	81 at%Al

The strong experimental variations of the penetration depths by small variations of the process parameters are not reproduced by the macro simulation. A reason for that may be the restrictions of the mixture concentration model. A tendency to stronger deviations with shorter interaction times is not observable (shorter interaction times would lead to less flow and bad mixing in the melt pool). However in earlier correlation series it was pointed out that reliably homogeneous mixing was achieved for  $\tau > 10$  ms [15]. In the macro simulations therefore convection should be considered additionally in future. Another explanation for the deviations may be the dependence of the absorption factor on temperature and iron concentration. This parameter could be measured for single laser treatments at high power. But at low power difficulties arise, when the temperature differences in calorimetric measurements are very small. Especially for cyclic treatments the absorption factor may change from the first to the second heat treatment, as the surface alloy

composition changes. Here reliable data are still missing and we notice that earlier correlations between the single remelting and simulations are clearly better [16].

Fig. 5 shows the calculated cooling rates for the sample in Fig. 4. The cooling rates in the solidification interval shows a maximum at the surface of the pool, which decreases to a minimum at the bottom of the pool. This corresponds with the refinement of the stem crystallites (Tab.1, Fig. 4). The following micro simulation is intended to examine the questions: Is the stem like morphology of the primarily formed  $\Theta$ -phase and the tendency of decreasing stem thickness from surface to bottom reproduced?

---

### Correlation between microstructure simulation and experiment

---

According to Fig. 5 cooling rate and temperature gradient were taken at different points of the solidification areas (above, center, down). They were used with the mixing concentration as input parameters for the microstructure simulations. Variations of numerical parameters, boundary conditions and the phase-field interface thickness  $\delta$  are not specified here for space reasons (more details in [16]). The grid resolution is  $\Delta x = 0.02 \mu\text{m}$  and  $\delta = 6 \Delta x$ .

In Fig. 4 also the results of the micro simulations under the three different local solidification conditions are shown. The grey scale represents the aluminum concentrations from 75 to 95%. Dark areas ( $c=75\%$ ) correspond to the solidified  $\Theta$ -phase. The crystallographic preferred direction is oriented in each case parallel to the temperature gradient. The boundary conditions are periodically selected from west to east and symmetrically for north and south.

All simulations start with a slightly disturbed planar front, which evolves to stem like microstructures. As in the experiment, no sidebranches are formed. The direct interaction of the diffusion fields on the tip level classifies the growth rather to cellular than dendritic. The selection of primary spacing is obviously not yet finished (the calculations must be repeated on a larger domain). Nevertheless the stem thicknesses reach values of ca.  $1\text{-}2 \mu\text{m}$  and are a bit thicker than the experimental values. Apart from this good agreement the simulations tend to select finer structures for higher cooling rates and so seem to reproduce the experimental decrease from bottom to top. It should be mentioned, that changes of the crystal orientation result in remarkable morphology changes in the simulations. Further statements from Figure 4 require more reliable results from the macro simulation and additional (larger) micro simulations.

Anyway this results of the micro simulation are encouraging us, because they seem to agree with the experiment much better than the correlation between macro simulation and experiment (see section 5.1). Since we found agreement on macroscale for this single specimen, the use of data from the macro simulation in this case seems legitime.

Fig. 6 shows the sensitivity of the simulation with increased aluminum concentration (84% instead of 80%). All other parameters are repeated like the simulations in Fig. 4 (for the area near to the surface). One stock grows out to a dendrite from the initially formed cellular structure. Also initial side branches are builded now.

---

### Outlook

---

In the further research project Fe-Al samples will be remelted also by pulsed laser processing. The investigations showed, that the absorption behavior is influenced strongly by the surface quality of the samples. This problems combined with low initial absorption for laser radiation may be reduced during pulsed laser radiation.

Additional simulations on macro-level are needed, if a better knowledge of the absorption coefficients is given. Moreover the Marangoni convection will be modeled in the future.

The micro simulations will be executed systematically to quantify the dependencies on local solidification parameters and numerical influences. Calculations in three dimensions are in work.

---

## Acknowledgements

---

This research project is funded by the DFG within the program "Kurzzeitmetallurgie" under Grant Number HE-2700/2-3

## References

---

- [1] W. Kurz, D.J. Fisher (1989) Fundamentals of Solidification, Trans Tech Publications, 3. Aufl., Aedermannsdorf.
- [2] E. Schubert, H.W. Bergmann (1993) Rapidly solidified surface layers by laser melting, Liebermann, Howard H.: Rapid solidified alloys, New York.
- [3] C. Beckermann, C.Y. Wan (1995) Multiphase /-scale modeling of alloy solidification, Annual Revue of Heat Transfer, V for this single specimen Vol VI, ed. L.I. Tien
- [4] G. Laschet, J. Neises and I. Steinbach (1998) Micro- and Macrosimulation of casting processes, 5ieme école d'été, Porquerolles, pp 1-42
- [5] R. Kobayashi (1993) Modeling and numerical simulations of dendritic crystal growth, Physica D, Vol 63, pp 410-423
- [6] A.A. Wheeler, B.T. Murray and R.J. Schaefer (1993) Computation of dendrites using a phase field model, Physica D 66, pp 243-262
- [7] S.-L. Wang et. al (1993) Thermodynamically consistent phase-field models for solidification, Physica D 69, pp 189-200
- [8] J. A. Warren, W.J. Boettinger (1995) Prediction of dendritic growth and microsegregation patterns in a binary alloy using the phase-field method, Acta metall.Mater. 43,2, pp 689-703
- [9] I.Steinbach et al.(1996) A phase field concept for multiphase systems,Physica D94,pp135-147
- [10] A. Karma, W-J. Rappel (1996) Phase field method for computationally efficient modeling of solidification with arbitrary interface kinetics, Phys Rev 53E, ppR3017-3020
- [11] A. Karma, W-J. Rappel (1997) Phase-field simulations of three dimensional dendrites: is microscopic solvability theory correct?, J. Cryst. Growth, 174, pp 54-64
- [12] C. Beckermann, H.-J. Diepers, I. Steinbach, A. Karma, X. Tong (1999) Modeling melt convection in phase-field simulations of solidification, J. Comp. Phys., 154, pp 468-496
- [13] J. Tieden, B. Nestler, H.J. Diepers, I. Steinbach (1998) The multiphase- field model with an integrated concept for modelling solute diffusion, Physica D 115, pp 73-86
- [14] Steinbach, G.J. Schmitz (1998) Direct numerical simulation of solidification structure using the phase field method, Proc. Modeling of Casting, Welding and Advanced Solidification Processes, TMS-edition, San Diego
- [15] G. Laschet, H.-J. Diepers, R. Prieler, I. Steinbach (1998) Micro-Macrosimulation of Laser Remelting of an Aluminium Coating on Steel, Proc. ECLAT'98, Ed. Mordike, B.L., Werkstoff-Informationsgesellschaft, 265-270
- [16] G. Laschet, H.-J. Diepers, R. Prieler, I. Steinbach (1997) Numerische Modellierung der Gefügebildung bei der Kurzzeitwärmebehandlung von Legierungen im System Fe-AL, ACCESS.

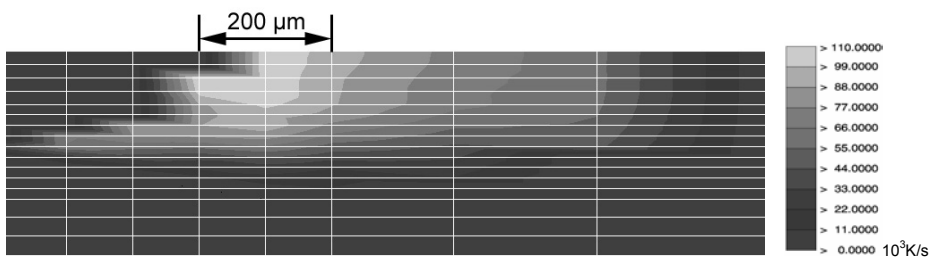


**Figure 5:** Cooling rates in the solidification intervall of Fig. 4. (Section in feed direction).



**Figure 6:** enhanced Al-content (85%)  
Other conditions see Fig. 4 (upper case).

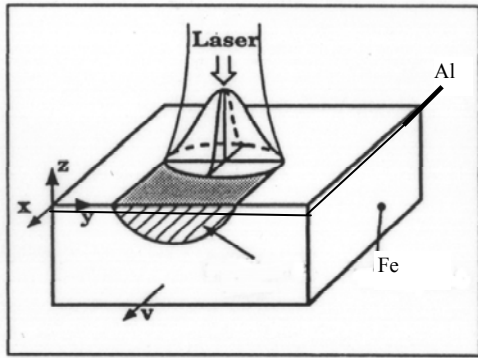


**Figure 1:** Scheme of the laser treatment

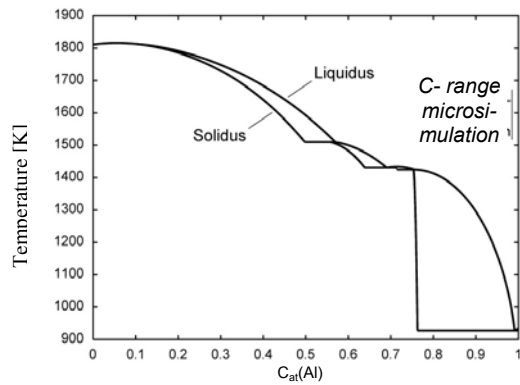


**Figure 3:** Liquidus and solidus curves in the phase diagram Fe-Al as extracted from ThermoCalc.

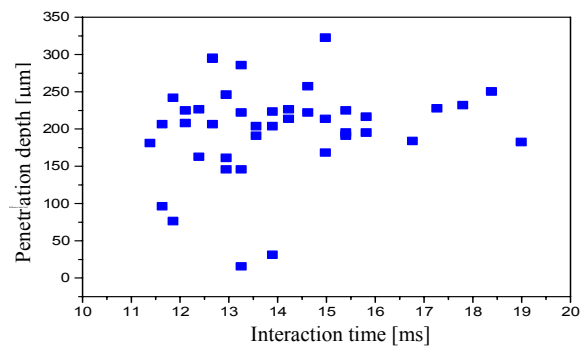
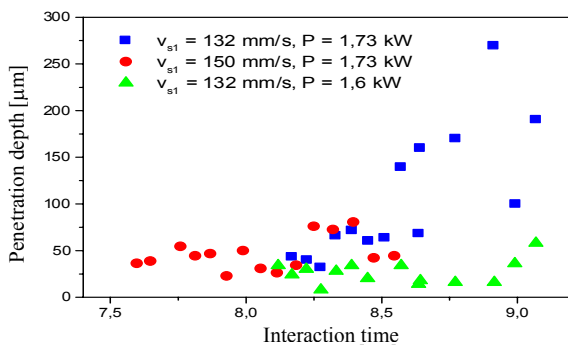


**Figure 2:** Experim. penetration depths in dependence on the (summed) interaction time for cyclic heat treatments. Three different laser velocities during the 1<sup>st</sup> treatment were applied.

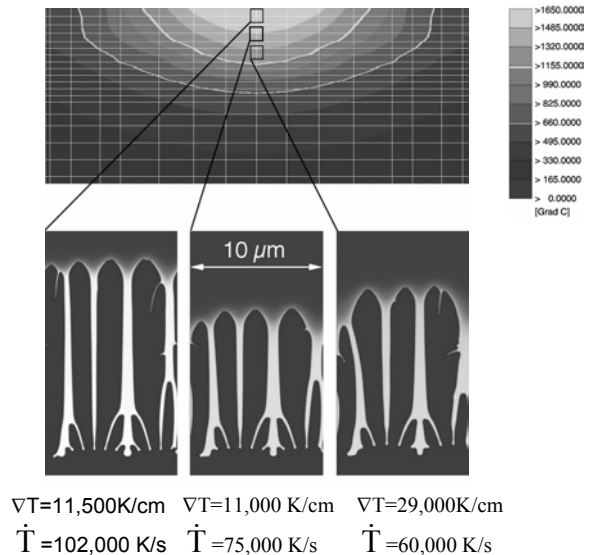
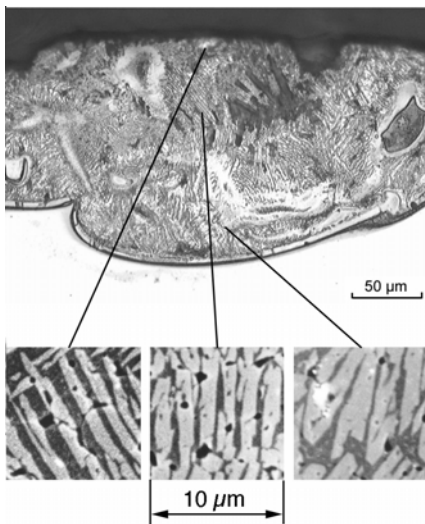


**Figure 4:** Comparison between experiment and simulation on macro- (up) and micro-scale (down). The liquidus and solidus isotherms for a calculated  $C_{Al} = 79.2$  at% are drawn within the temperature distribution in cross section. The liquid reaches a depth of  $175 \mu\text{m}$ . At different positions the subsequent micro simulations show a slightly different selection with tendency to finer micro structures at higher cooling rates (higher positions). The grey scale indicates the Al concentration (75%-95%), so dark identifies solid.